Revue Roumaine de Chimie, **2006**, *51*(11), 1095–1108

COMPARISON OF VACUUM SWING ADSORPTION PROCESS[1] FOR AIR SEPARATION USING ZEOLITE 10X AND 13X

Jeong-Geun JEE,[a] Jin-Hwan JUNG,[b] Jae-Wook LEE,[c] Soong-Hyuck SUH[d] and Chang-Ha LEE[b*]

[a] Samsung Electronics Co., Ltd., Yongin 449-711, Korea
[b] Department of Chemical Engineering, Yonsei University, Seoul 120-749, Korea
[c] Department of Chemical Engineering, Seonam University, Namwon 590-711, Korea
[d] Department of Chemical Engineering, Keimyung University, Daegu 704-701, Korea

Received February 7, 2006

The five-step two-bed vacuum swing adsorption (VSA) process for air separation was investigated both experimentally and theoretically. The adsorption characteristics and dynamics of the bed packed with zeolite 10X or 13X were compared and the performance of the VSA process with each adsorbent was presented. A non-isothermal dynamic model incorporating mass and energy balances was applied to predict the process dynamics using the linear driving force (LDF) model and the loading ratio correlation (LRC) isotherm. The adsorption amount of N_2 and O_2 on zeolite 13X was higher than that on zeolite 10X while the selectivity of both adsorbents was similar. However, the high bed porosity of zeolite 13X bed had a detrimental effect on the process performance. The step-time of adsorption and pressure equalization steps in the VSA affected significantly the O_2 purity and recovery while that of pressurization step was negligible. In addition, the vacuum pressure during desorption step step proved to be one of the key factors in the process performance. Finally, the VSA using zeolite 10X produced a purity level of 92% O_2 with 70+% recovery while the VSA using zeolite 13X produced a O_2 product with 90% purity and 50+% recovery due to the high bed porosity. However, the productivity of both VSA processes was similar to each other because the net loading of zeolite 13X in the bed was relatively small.

INTRODUCTION

In the field of air separation, the classical cryogenic distillation has been recognized as one of the most common methods of oxygen production. However, this technology is not competitive for relatively small size oxygen plants *i.e.*, less than 100TPDc (tons per day contained) oxygen.[1]

Recently, the development of highly selective adsorbents such as LiX, LiAgX, and LiCaX has contributed to the possibility of manufacturing up to 200 TPDc by vacuum swing adsorption (VSA) process, at a power consumption rate competitive with that of cryogenic distillation.[2-3] Moreover, VSA process for air separation is competitive with pressure swing adsorption (PSA) process for the production of over 15 TPDc oxygen.[1]

Most VSA processes for air separation are generally operated in the range of 1.1 to 1.8atm adsorption pressure and 0.05 to 0.3atm desorption pressure.[1,3,4~7] The low adsorption pressure which slightly exceeds the ambient pressure enables the use of blower as the supplier of air instead of the expensive compressor while the additional vacuum pump was needed. Therefore, the optimum desorption pressure plays a key role in reducing both the energy and the equipment cost. In addition, each step time of VSA process and adsorbent capacity are important factors to maximize the process performance.

[1] To whom the correspondence should be addressed: e-mail: leech@yonsei.ac.kr.

Budner et al. and Sircar *et al.*[3,6] reported that zeolite CaX shows a high selectivity for nitrogen over oxygen. However, zeolite NaX has been widely used as both the main and pretreatment adsorbent[1] because zeolite CaX shows weak chemisorption with water. Jee et al.[8] investigated the adsorption dynamics of various adsorbents for air separation. They reported that the adsorption dynamics of each bed were different due to tailing effect and temperature variation.

In this study, the VSA process packed by zeolite 10X or 13X, which is widely used in commercial VSA process for air separation, was compared with each other. The process performance was optimized through the experimental and theoretical works with respect to the purity, recovery, and productivity. A non-isothermal dynamic model incorporating mass, energy, wall-energy balances was applied to predict the process dynamics. The linear driving force (LDF) model and the Langmuir-Freundlich isotherm were used for the adsorption rate and equilibrium, respectively.

MATHEMATICAL MODEL

To understand the dynamic behaviors of the adsorption bed during the VSA running, the mathematical models were developed on the basis of the following assumptions: (i) the gas phase behaves as an ideal gas mixture, (ii) radial concentration and temperature gradients are negligible, (iii) thermal equilibrium between adsorbents and bulk flow is assumed, (iv) the flow pattern is described by the axially dispersed plug flow model, (v) the mass transfer rate is represented by a LDF model, (vi) the heat capacities are constant and the heat capacity of adsorbed phase is negligible,[12] and (vii) the pressure drop along the bed is negligible.[13,14] The assumption of neglecting radial gradient was widely accepted by numerous studies, and the others are also common assumptions in simulating the adsorption process.[7,8,15]

The heat of adsorption varies with the surface coverage. However, because the variation of heat of adsorption is small in the experimental range, it is assumed to be constant in the study.[11, 24-27]

The component and overall mass balances for the bulk phase in the adsorption column are given by

$$-D_L \frac{\partial^2 c_i}{\partial z^2} + \frac{\partial (u c_i)}{\partial z} + \frac{\partial c_i}{\partial t} + \rho_p \left(\frac{1-\varepsilon}{\varepsilon} \right) \frac{\partial \overline{q_i}}{\partial t} = 0 \tag{1}$$

$$\frac{\partial (uC)}{\partial z} + \frac{\partial C}{\partial t} + \rho_p \left(\frac{1-\varepsilon}{\varepsilon} \right) \sum_{i=1}^{n} \frac{\partial \overline{q_i}}{\partial t} = 0 \tag{2}$$

Another characteristic of the adsorption process is the temperature variation caused by the heat of adsorption and desorption. To minimize the deviation in the prediction of high purity product, the energy balance for the gas phase also includes the heat transfer to the column wall.

$$\begin{aligned} &-K_L \frac{\partial^2 T}{\partial z^2} + \varepsilon \rho_g C_{pg} \frac{\partial (uT)}{\partial z} + \left(\varepsilon_t \rho_g C_{pg} + \rho_B C_{ps} \right) \frac{\partial T}{\partial t} \\ &- \rho_B \sum_{i=1}^{n} \left(-\Delta \overline{H_i} \right) \frac{\partial \overline{q_i}}{\partial t} + \frac{2h_i}{R_{Bi}} (T - T_w) = 0 \end{aligned} \tag{3}$$

Where, ε_t is the total void fraction (= $\varepsilon + (1 - \varepsilon) \times \alpha$), α is the particle porosity, and ρ_B is the bed density, (= $(1 - \varepsilon) \times \rho_p$).

In order to consider the heat loss through a wall and the heat accumulation in the wall, another energy balance for the wall of the adsorption bed was used.

$$\rho_w C_{pw} A_w \frac{\partial T_w}{\partial t} = 2\pi R_{Bi} h_i (T - T_w) - 2\pi R_{Bo} h_o (T_w - T_{atm}) \tag{4}$$

where, $A_w = \pi (R_{Bo}^2 - R_{Bi}^2)$

The boundary and initial conditions of mass and energy balances are presented below. The well-known Danckwerts boundary conditions are applied.[16]

<Boundary conditions for feed pressurization (PR) and adsorption (AD) steps>

$$-D_L\left(\frac{\partial c_i}{\partial z}\right)\Big|_{z=0} = u(c_i|_{z=0^-} - c_i|_{z=0^+}) \quad ; \quad \left(\frac{\partial c_i}{\partial z}\right)\Big|_{z=L} = 0 \tag{5a}$$

$$-K_L\left(\frac{\partial T}{\partial z}\right)\Big|_{z=0} = \varepsilon\rho_g C_{pg} u(T|_{z=0^-} - T|_{z=0^+}); \quad \left(\frac{\partial T}{\partial z}\right)\Big|_{z=L} = 0 \tag{5b}$$

Where, $y_i|_{z=o^-}$ means feed composition for component *i*.

<Boundary conditions for pressurizing pressure equalization (PPE) step>

$$-D_L\left(\frac{\partial c_i}{\partial z}\right)\Big|_{z=L} = u(c_i|_{z=L^+} - c_i|_{z=L^-}) \quad ; \quad \left(\frac{\partial c_i}{\partial z}\right)\Big|_{z=0} = 0 \tag{6a}$$

$$-K_L\left(\frac{\partial T}{\partial z}\right)\Big|_{z=L} = \varepsilon\rho_g C_{pg} \quad u(T|_{z=L^+} - T|_{z=L^-}) \quad ; \quad \left(\frac{\partial T}{\partial z}\right)\Big|_{z=0} = 0 \tag{6b}$$

Where, $y_i|_{z=L^+}$ means a temporal effluent's composition during a depressurizing pressure-equalization step for the pressurizing pressure-equalization step. The fluid velocity is inherently negative during this step.[16]

<Boundary conditions for depressurizing pressure equalization (DPE) and countercurrent vacuum regeneration (VU) steps>

$$\left(\frac{\partial c_i}{\partial z}\right)\Big|_{z=0} = \left(\frac{\partial T}{\partial z}\right)\Big|_{z=0} = 0 \quad ; \qquad \left(\frac{\partial c_i}{\partial z}\right)\Big|_{z=L} = \left(\frac{\partial T}{\partial z}\right)\Big|_{z=L} = 0 \tag{7}$$

Also, the boundary conditions for interstitial velocity in each step are presented below.

<Boundary conditions for interstitial velocity>

$u|_{z=0} = 0$ (Depressurizing and pressurizing pressure equalization steps)

$u|_{z=N} = 0$ (Pressurization and Vacuum steps)

$$u|_{z=0} = u_{feed} \quad \text{(Adsorption step)} \tag{8}$$

In this study, the pressure history at the product end during a VSA experiment was fitted by the following 5th order polynomials and the equation was used as a boundary condition for the overall mass balance.

$$P = at + bt^2 + ct^3 + dt^4 + et^5 \tag{9}$$

The multi-component adsorption equilibrium was predicted by the following LRC model:

$$q_i = \frac{q_{mi} B_i P_i^{ni}}{1 + \sum_{j=1}^{n} B_j P_j^{nj}} \tag{10}$$

The sorption rate into an adsorbent pellet is described by the LDF model with a single lumped mass transfer parameter:[17]

$$\frac{\partial \overline{q_i}}{\partial t} = \omega_i \left(q_i^* - \overline{q_i} \right) \quad , \quad \omega_i = \frac{KD_{ei}}{r_c^2} \tag{11}$$

The adsorption isotherm parameters and LDF coefficients of N_2, O_2, and Ar on zeolite 10X and 13X are listed in Table 1. The adsorbed amounts of N_2, O_2, and Ar on zeolite 10X and 13X in this study **display** similar values compared with the published equilibrium data.[8]

Table 1

Equilibrium/rate parameters and heat of adsorption of N_2, O_2, and Ar for zeolite 10X and zeolite 13X.

Adsorbent	Zeolite 10X			Zeolite 13X		
Adsorbate	N_2	O_2	Ar	N_2	O_2	Ar
$q_m * 10^3$(mol/g)	1.0181	1.3748	2.2033	2.2399	0.9953	0.9633
$B*10^2(1/atm^n)$	28.005	6.8999	3.0520	17.020	13.227	12.367
n(-)	0.9074	0.8775	0.9516	0.9771	1.0577	1.0109
Heat of adsorption, $-\Delta\bar{H}$ (Cal/mol)	3900	2300	2300	4100	2600	2500
LDF coefficient, ω_i (s^{-1})	0.065	0.23	0.22	0.09	0.25	0.22

EXPERIMENTAL

A schematic diagram of the breakthrough apparatus is shown in Fig. 1. The adsorption bed was made of stainless-steel pipe with a length of 100cm, a ID of 2.2cm, and a wall thickness of 0.175 cm. Zeolite 10X (Baylith, WE-G 639) and 13X (Baylith, WE-G 652) were used as adsorbents. Prior to each experimental run, the adsorbent was regenerated at 613K over night. The characteristics of adsorbent and adsorption beds are listed in Table 2.

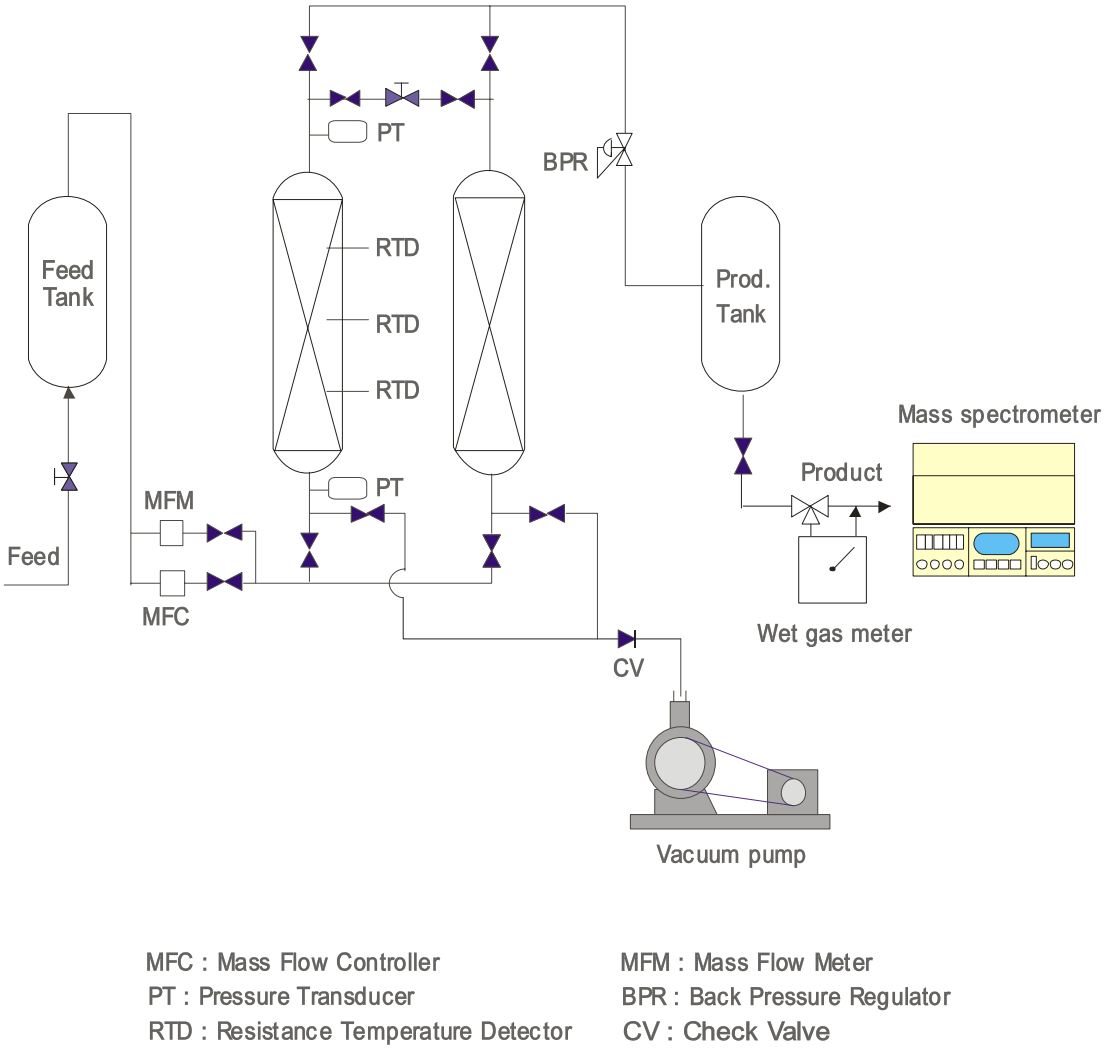

Fig. 1 – Schematic diagram of apparatus for a two-bed O_2 VSA process.

Table 2

Characteristics of adsorbents and adsorption bed.

Adsorbent	Zeolite 10X	Zeolite 13X
Type	Sphere	Sphere
Average pellet size, R_p [cm]	0.115	0.1
Pellet density, ρ_p [g/cm^3]	1.1	1.03
Heat capacity, C_{ps} [cal/g·K]	0.27	0.32
Particle porosity, α [-]	0.36	0.35
Bed density, ρ_B [g/cm^3]	0.82	0.695
Adsorption Bed		
Length, L [cm]	100	
Inside radius, R_{Bi} [cm]	1.7	
Outside radius, R_{Bo} [cm]	1.875	
Heat capacity of column, C_{pw} [cal/g·K]	0.12	
Density of column, ρ_w [g/cm^3]	7.83	
Internal heat transfer coefficient, h_i [cal/cm^2·K·sec]	9.2E-4	
External heat transfer coefficient, h_o [cal/ cm^2·K·sec]	3.4E-4	
Axial thermal conductivity, K_L [cal/cm·sec·K]	6.2E-5	
Axial dispersion coefficient, D_L [cm^2/sec]	1.0E-5	

Three calibrated resistance temperature detectors (RTD, Pt 100Ω) were installed at the positions of 10, 50, and 80cm from the feed end and at the center of radial position in order to measure the temperature variations inside the bed. The two pressure transducers were located at the feed and product ends in order to measure the bed pressure variation and the degree of pressure drop inside the bed. The feed flow rate was controlled by a mass flow controller (Hastings, 202D-799). And the surge tank of the same size as the adsorption bed was equipped to prevent flow fluctuation. The total amount of feed flow and the flow rate of each step were measured by a wet gas meter. In order to keep the pressure in the adsorption bed constant, an electric back pressure regulator was installed between the adsorption bed and the product bed. The high performance vacuum pump (Ulvac, DAH-60) was used to evacuate the adsorption bed in the range of 0.2 to 0.4atm during the vacuum step. The concentration variations of the influent and effluent were analyzed by a quadrupole mass spectrometer (Pfeiffer Vacuum, QMG 422). This mass spectrometer has its own error in the range of ±0.1% at every run. The calibration by gas chromatographs (HP 5890, series II) was conducted before each process run.

The system was fully automated by a personal computer with a developed control program and all measurements including pressure, temperature, and O_2 purity were saved on the personal computer through the AD converter.

The ternary mixture (N_2/O_2/Ar; 78/21/1 vol. %) assumed as the composition of ambient air was used as a feed gas for the VSA experiments. The adsorbent was regenerated at 613K over night. The bed packed with the adsorbent was kept at a 1.8atm pure O_2 (99.9+%) condition to prevent contamination from the outside air. Prior to each experimental run, the adsorption bed was vacuumed up to 9 torr for 2 hours. And, before each experimental run, the adsorption bed was pressurized at 1.8atm using pure oxygen and was kept for 1 hour. The temperatures of feed, bed, and surroundings as the initial experimental temperature were kept in the range of 298K to 299K. The process performances were studied in the range of cycle time of 146-210sec under the adsorption pressure of 1.8atm and the feed flow rate in the range of 1.3- 2.8LSTP/min. Therefore, the high and low pressure limits in this study were fixed as 1.8atm for the adsorption step and 0.2 to 0.4atm for the vacuum step, respectively. The more detailed operating conditions are shown in Table 3.

Table 3

Operating conditions for VSA experiments

Run No.	Adsorbate	Studied Variables	Feed flow rate [LSTP/min.]	Vacuum pressure [atm]	Step time [sec] (PR-AD-DPE-VU-PPE)
1	Zeolite 10X	AD step	1.3	0.32	40-**25**-25-**65**-25
2				0.30	40-**30**-25-**70**-25
3				0.28	40-**35**-25-**75**-25
4				0.26	40-**40**-25-**80**-25
5		PR step	1.3	0.40	**20**-30-25-**50**-25
6				0.34	**30**-30-25-**60**-25
7		PE step	1.3	0.30	40-30-**8**-70-**8**
8					40-30-**15**-70-**15**
9		Feed flow rate	**2.1**	0.30	40-30-25-70-25
10			**2.8**		
11	Zeolite 13X	AD step	1.3	0.28	40-**15**-25-**55**-25
12				0.26	40-**20**-25-**60**-25
13				0.24	40-**25**-25-**65**-25

Table 3 (continues)

Table 3 (continued)

14				0.22	40-**30**-25-**70**-25
15		PR step	1.3	0.29	**20**-30-25-**50**-25
16				0.26	**30**-30-25-**60**-25
17		PE step	1.3	0.22	40-30-**8**-70-**8**
18					40-30-**15**-70-**15**
19		Feed flow rate	**2.1**	0.22	40-30-25-70-25
20			**2.8**		

The five step two-bed VSA process without purge step was employed to obtain high purity oxygen from air. The five-step used is as follows: (I) cocurrent feed pressurization (PR) of a partially pressurized bed by a previous pressurizing pressure equalization step (PPE), (II) high-pressure adsorption (AD) step, (III) cocurrent depressurizing pressure equalization (DPE) step, (IV) countercurrent vacuum (VU) step, and (V) countercurrent pressurizing pressure equalization (PPE) step. A cyclic sequence of a five-step two-bed VSA process is listed in Table 3 and it was described **in** previous works in detail.[7, 21]

RESULTS AND DISCUSSION

The adsorption isotherms of N_2, O_2, and Ar on zeolite 10X and 13X at 293.15K are shown in Fig. 2. The equilibrium selectivity between N_2 and O_2 is prominent from sub-ambient pressure (about 0.2atm) to high pressure (2atm). The isotherms imply that zeolite 10X and 13X cannot separate argon from oxygen because of almost same adsorption amount. However, the adsorption capacity of N_2 was about three times larger than those of O_2 and Ar.

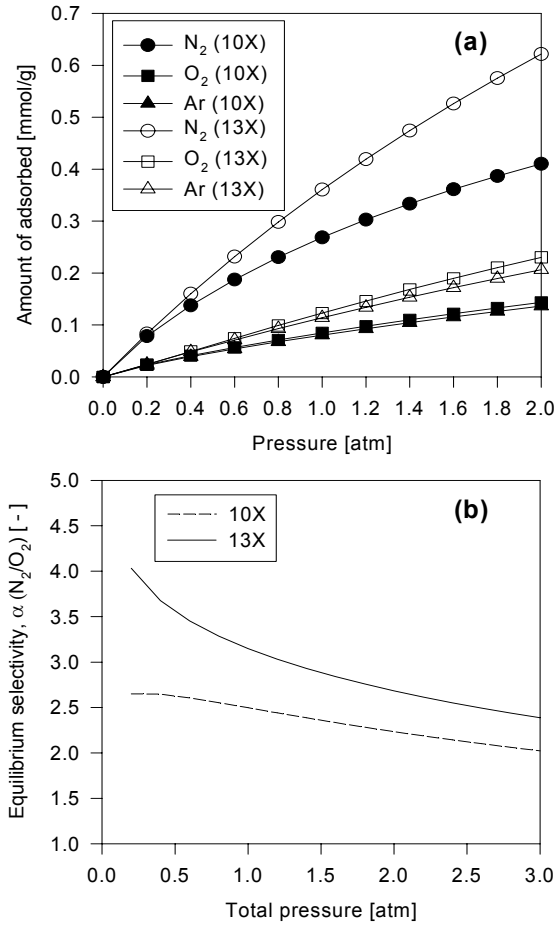

Fig. 2 – Adsorption isotherms of O_2, N_2, and Ar on (a) zeolite 10X and (b) zeolite 13X at 293.15K.

The net adsorption amounts of N_2 and O_2 on zeolite 13X were higher than those on zeolite 10X with an increase in adsorption pressure while the difference of selectivity between zeolite 13X and 10X was small. As represented in Table 2, it is expected that the process performance of zeolite 13X may be worse than that of z**eo**lite 10X due to the low bulk density of zeolite 13X. A low porosity in bed means a higher adsorbent content and a higher adsorption capacity. In addition, it leads to less loss of the adsorbable component during the depressurization step and less amount of product gas for an effective extraction during the regeneration step.

The accurate pressure variation data in the packed bed is prerequisite to decide the vacuum step time of VSA process. Prior to the VSA experiment, the pressure variation through the vacuum step time was examined by using the vacuum pump with the capacity of 60 l/min. As a result, 50 to 70sec was needed to reach the desired desorption pressure, about 0.3atm, from ambient pressure. The zeolite 13X bed with high bed porosity reached slightly faster the aim desorption pressure than the zeolite 10X bed as shown in Fig. 3.

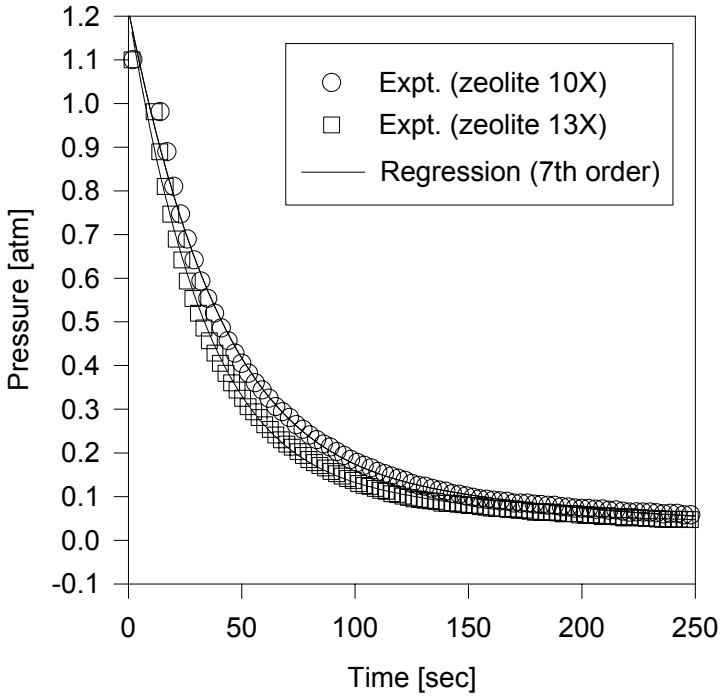

Fig. 3– Pressure variation and regression profile from ambient to vacuum pressure in the beds packed with zeolite 10X or 13X.

As the concentration wave fronts of N_2 and O_2 propagated along the bed, the heat of adsorption caused a temperature rise in the bed. Temperature histories at 10, 50, and 80 cm from the feed end under the 30sec adsorption step time (Run. 2 and Run. 14) are presented in Fig. 4. Because of large amount of adsorption and heat of adsorption, the temperature variation of zeolite 13X bed was higher than that of zeolite 10X bed. However, as can be seen in Fig. 4, the temperature excursion was about 2-3K at the feed end. Therefore, the selectivity change of zeolite 10X and 13X by the heat of adsorption is almost negligible. It implies that the system behaves almost isothermal, as was observed **by** Kapoor and Yang[19] and Mendes et al.[21]

Fig. 5 shows a representative cyclic behavior by comparing the experimental concentration with the predicted concentration variation. After approximately 16 to 18 cycles, the performance difference between the last two cycles was less than 0.05%. Therefore, in the present study, all the VSA experimental data were collected at above 20 cycles as the result of cyclic steady-state.

The effects of adsorption step time on the O_2 purity and recovery are shown in Fig. 6. As shown in Fig. 6(a), the purity was decreased as the AD step times increased. It was because the increased AD step time led to a breakthrough of N_2 toward the product end. However, the purity was somewhat broadly decreased because the increased AD step time led to an increased VU step time and a decrease of desorption pressure as shown in Fig. 6(b).

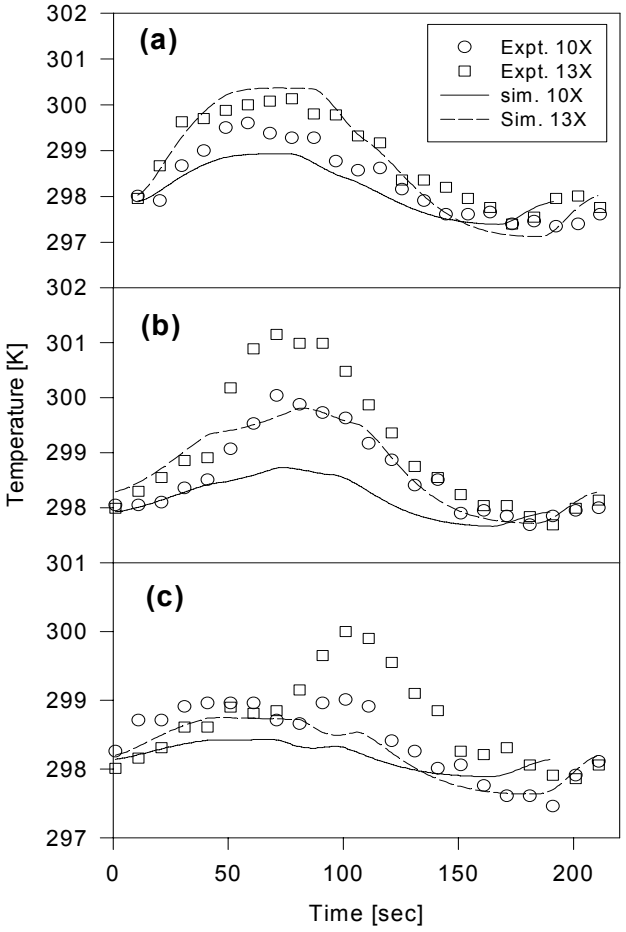

Fig. 4 – Experimental and simulated temperature curves of zeolite 10X and 13X beds at the position of (a) 10cm, (b) 50cm, and (c) 80cm from the feed end at 1.8atm and 1.3LSTP/min.

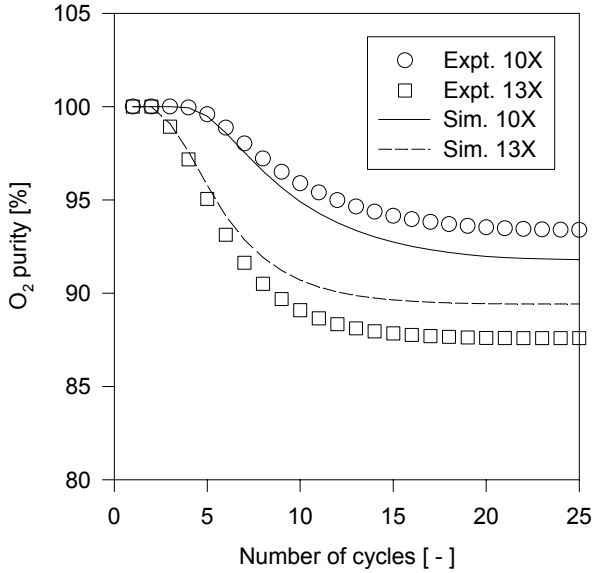

Fig. 5 – Variation of product purity from cyclic unsteady-state to steady-state.

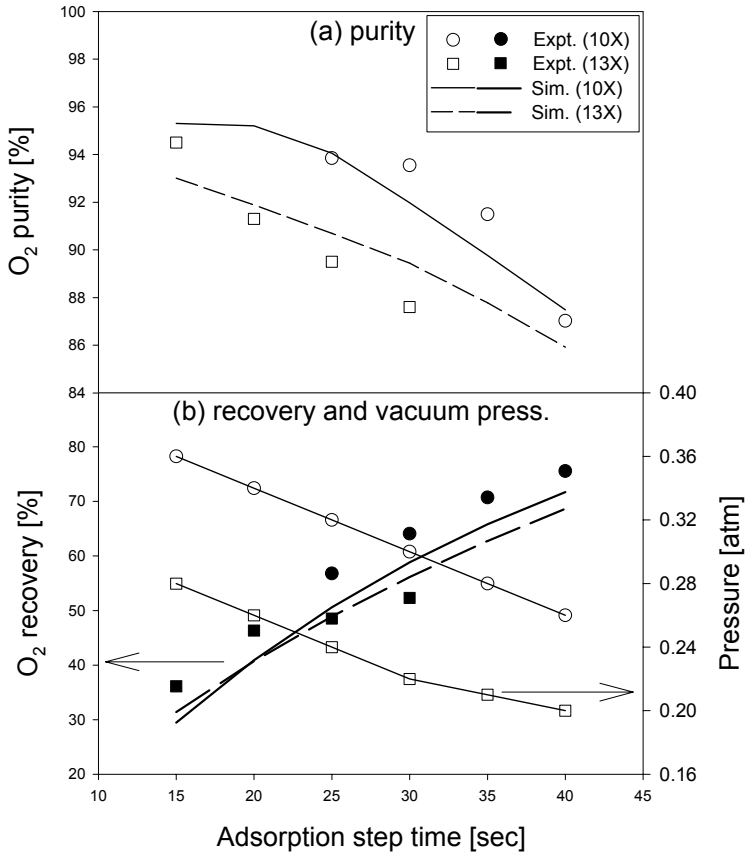

Fig. 6 – Effect of adsorption step time on the (a) O_2 purity and (b) O_2 recovery and pressure variation profile during vacuum step (From runs 1 to 4).

Zeolite 10X bed produced higher purity oxygen than zeolite 13X bed at all the conditions of the experimental adsorption step times. However, the difference between zeolite 10X and 13X beds was broadly decreased as the AD step time increased. It was because the desorption pressure of zeolite 13X bed reached 0.2atm, which seems to be a barrier pressure of VSA at the condition of 40sec AD step time. The results showed that the low bed porosity gave a detrimental effect on the adsorption capacity of zeolite 13X bed regardless of its adsorption isotherm. As can be seen in Fig. 6(b), the recovery increased almost linearly with an increase in the AD step time because the increased adsorption step time caused the increase of net amount of product. In addition, the recovery of zeolite 10X bed was higher than that of zeolite 13X bed. However, at the condition of short AD step time from 15 to 20sec, the recovery difference between zeolite 10X and 13X beds was nearly negligible or showed even crossover. In sum, the VSA process using zeolite 10X could produce 92% oxygen with 70% recovery while the zeolite 13X VSA could produce 90% oxygen with 50% recovery.

Such performance difference between these two processes can be explained by Fig. 7. In Fig. 7(a), the O_2 mole fraction at the product end of zeolite 10X bed was kept constant about 15sec regardless of the propagation of O_2 mass transfer zone (MTZ). However, after 15sec, the product end was gradually contaminated by the N_2 MTZ. Fig. 7(b) shows the MTZ variation of N_2 and O_2 in the zeolite 13X bed during the adsorption step time. The N_2 and O_2 MTZs of zeolite 13X bed were steeper than those of zeolite 10X bed while their moving velocity was faster than those of the zeolite 10X bed. These results stemmed from the isotherms and bed porosity, respectively.

The effect of pressurization step time on the purity and recovery is shown in Fig. 8. The purity and recovery were slightly increased with the PR step time because the increased PR step time led to a lower vacuum pressure of the other bed. However, the variation of purity and recovery with the PR step time was in the range of 1-3%. Therefore, the effect of PR step on the process performance was not significant in the operating ranges.

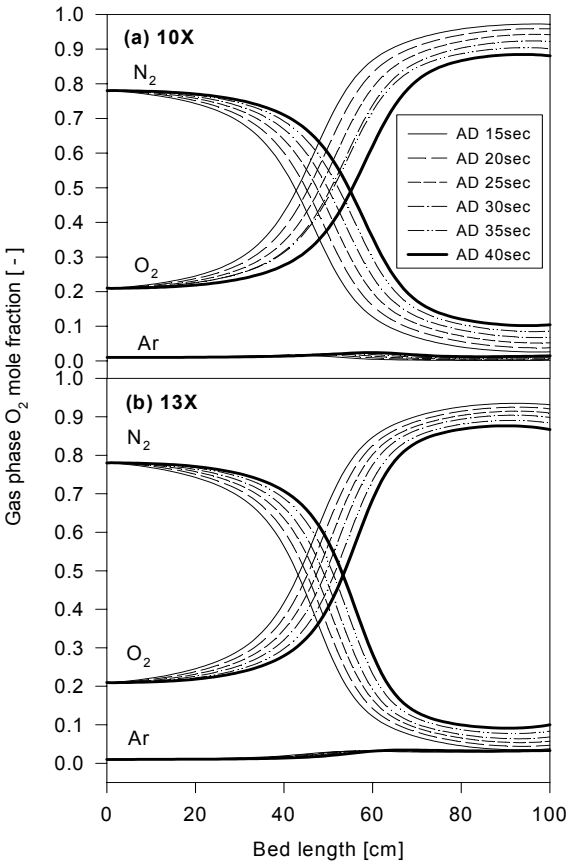

Fig. 7 – O_2 concentration profile along the bed during AD step at various adsorption step time.

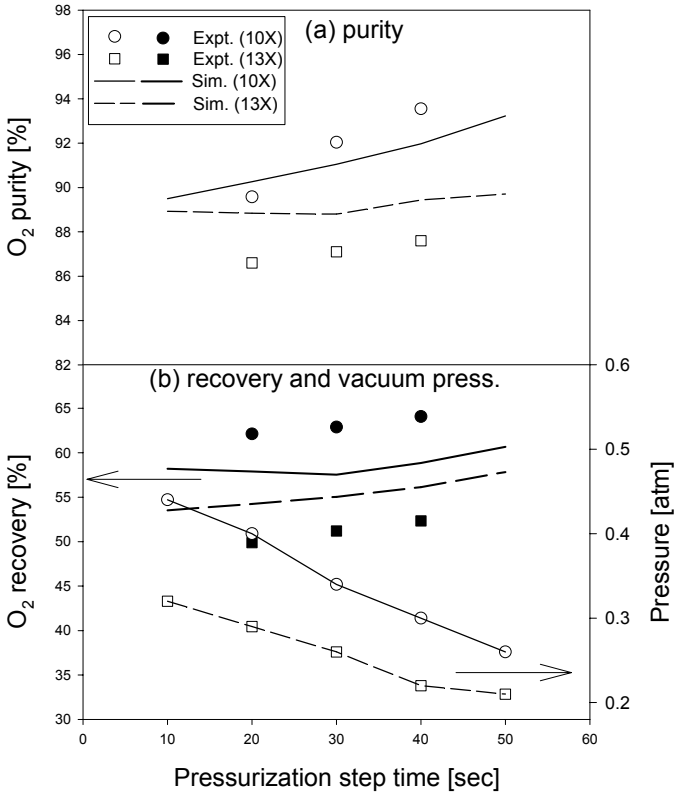

Fig. 8 – Effect of pressurization step time on the (a) O_2 purity and (b) O_2 recovery and pressure variation profile during vacuum step (From runs 1- 4, 11-14).

However, since the PR step was related to the VU step, the optimum PR step time should be decided to achieve high productivity as well as high purity oxygen production. As shown in Fig. 9, the convex shape MTZ was formed at the PR step. Although the MTZs at 40-50 sec were steeper and slightly farther from the product end than the MTZ at 10 sec, the product end was more contaminated at these longer PR step times. The O_2 MTZ in zeolite 13X bed in Fig. 9(b) was more closely approached to the product end than that in zeolite 10X bed in Fig. 9(a) because of its low packing density. However, the O_2 MTZ was steeper in zeolite 13X bed than in zeolite 10X bed because of its favorable isotherm shape.

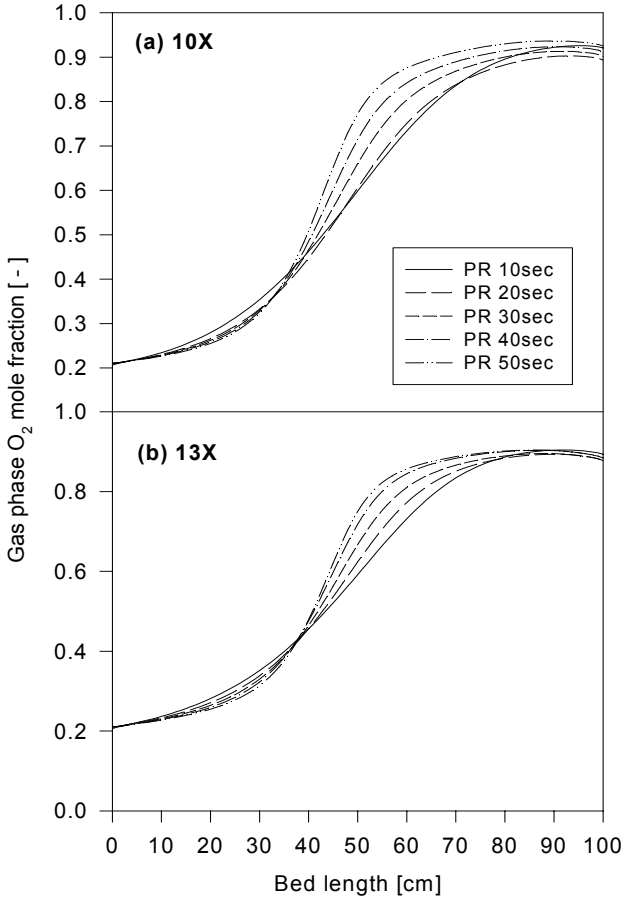

Fig. 9 – O_2 concentration profile along the bed during PR step at various adsorption step time.

The effect of pressure equalization step time on the purity and recovery is shown in Fig. 10. The purity and recovery were noticeably increased with the PE step time. The increased PE step time implies that the flow moves slowly to the other bed. Therefore, as the PE step time was increased, the nitrogen in adsorbed phase was slowly desorbed and the mole fraction of O_2 in the effluent would be increased. Especially, the purity between zeolite 10X and 13X beds was crossed over when the PE step time was below 10sec.

The results can be explained by Fig. 11. In Fig. 11(a) and (b), the slower flow rate at the DPE step caused the steeper O_2 MTZ. Moreover, the higher purity O_2 at this step was delivered to the other bed as shown in Fig. 11(c) and (d). In addition, the extended PE step time led to the higher O_2 recovery because the smaller amount of O_2 was vented at the blowdown step. Therefore, it caused both the steep O_2 MTZ in the PR step and the high O_2 purity in the AD step. However, the extents of the MTZ change with an increase in the DPE step time and PPE step time became smaller. Therefore, the PSA performance in Fig. 10 was asymptotically improved with the change of the PE step time. Furthermore, the O_2 MTZ of DPE and PPE steps in zeolite 10X bed was steeper at the condition of relatively long PE step time of 25-30 sec. On the contrary, as the PE step time was shortened, the difference between the two beds became smaller. As a result, the O_2 concentration of product end in the zeolite 13X bed was higher than that in the zeolite 10X bed at short PE time of 5-10sec.

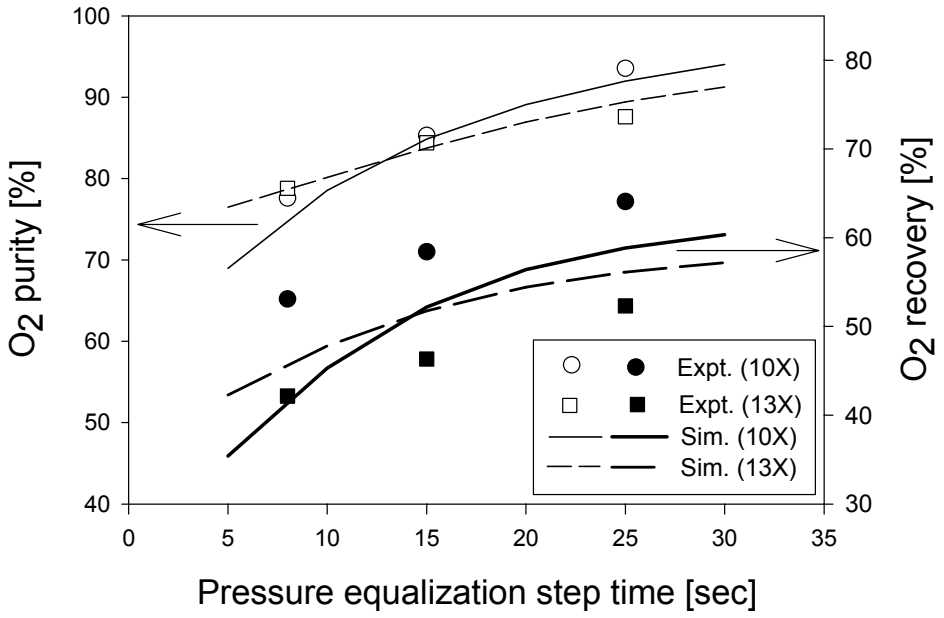

Fig. 10 – Effect of pressure equalization step time on the O_2 purity and recovery. (From runs 2, 7-8, 14, 17-18).

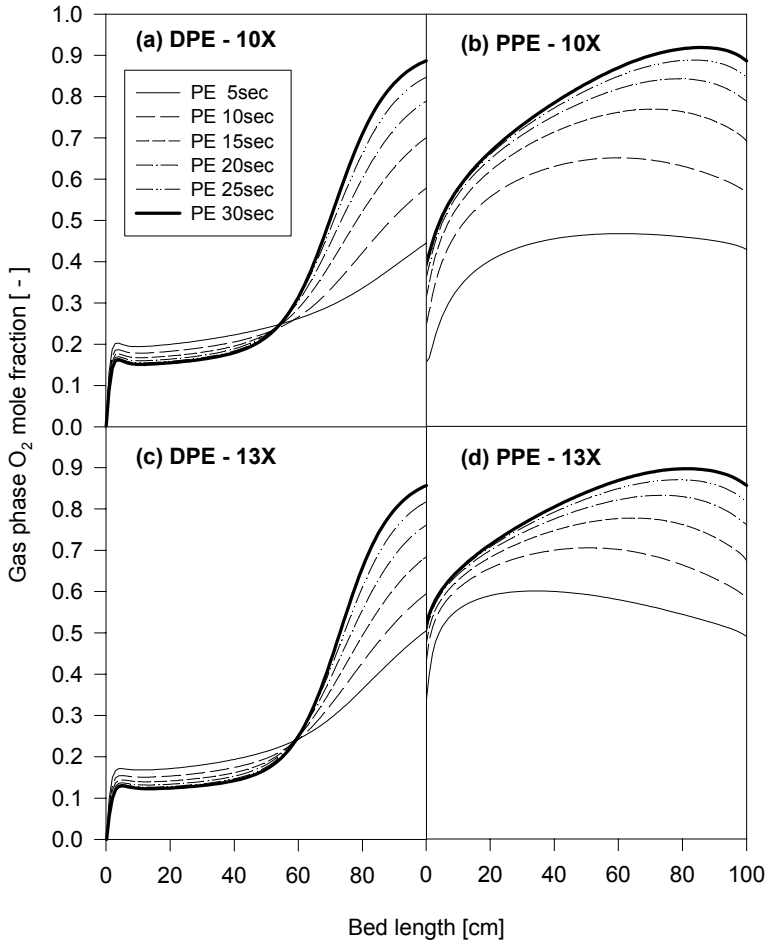

Fig. 11 – O_2 concentration profile along the bed during DPE and PPE steps at various adsorption step time.

The effect of feed flow rate on the purity and recovery is shown in Fig. 12. The purity and recovery were drastically decreased as the feed flow rate was increased. In addition, as similar to the effect of PE step times, the purity and recovery from zeolite 10X and 13X beds were crossed over as the feed flow rate was increased.

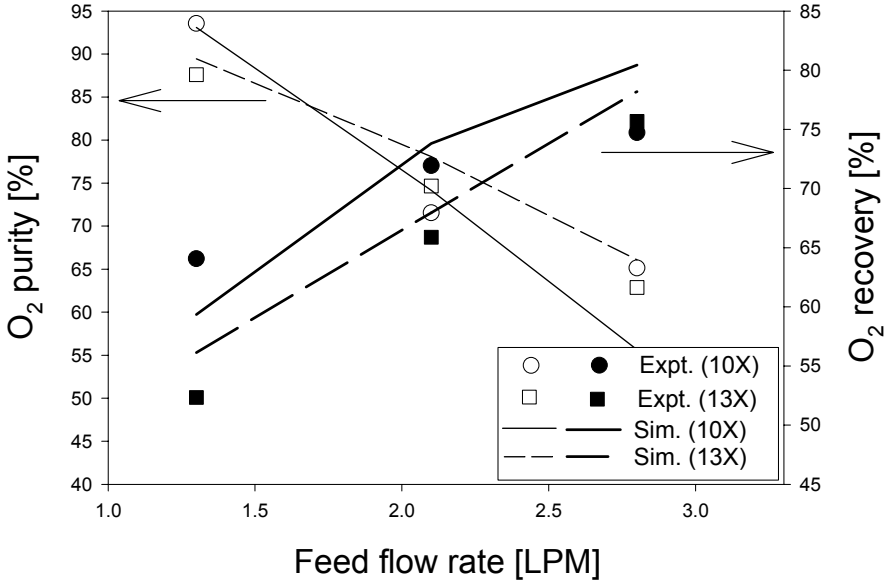

Fig. 12 – Effect of feed flow rate on the O_2 purity and recovery. (From runs 2, 9-10, 14, 19-20).

The productivities of the suggested VSA processes within the experimental operating ranges were 3.85×10^{-4}mmol/g sec for zeolite 10X and 3.67×10^{-4}mmol/g sec for zeolite 13X. The productivity of VSA process was higher than that of a conventional PSA process. In sum, the purity and recovery from the zeolite 10X VSA was higher than those from the zeolite 13X VSA, but the productivity between these two VSA processes was nearly same because of the difference of bulk density.

CONCLUSION

The effects of step time and operating variables on adsorption and desorption dynamics were studied for the five-step two-bed O_2 VSA with zeolite 10X or 13X.

The adsorption isotherms of O_2, N_2, and Ar on zeolite 10X and 13X were compared in the range of 0.2 to 2atm, which is generally regarded as the working condition of O_2 VSA. Though zeolite 13X showed the higher adsorption amount for each component in air, its lower bed porosity gave a detrimental effect on the performance of VSA process. In addition, the pressure decrease during vacuum step was affected by the bed porosity.

Temperature variation during the whole cycle was less than 3K in all the zeolite bed, showing slightly higher variation in zeolite 13X bed than in zeolite 10X bed. Therefore, all the beds could be assumed to isothermal condition because of its small heat of adsorption.

As the adsorption step time increased, the purity was decreased. However, the purity was somewhat broadly decreased because the desorption pressure was simultaneously decreased by the extended vacuum step time. Also, the purity and recovery of zeolite 10X bed were slightly higher than those of zeolite 13X bed at all the conditions of the applied adsorption step time. The O_2 purity was slightly increased with the pressurization step time because the increased pressurization step time led to the decrease of vacuum pressure. The pressure equalization step time and feed flow rate also had a great effect on purity and recovery. The crossover of purity and recovery between zeolite 10X and 13X VSA processes was observed by changing these both operating conditions.

In sum, the VSA process using zeolite 10X could produce 92% oxygen with 70% recovery while the zeolite 13X VSA could produce 90% oxygen with 50% recovery. However, the productivity between these two VSA processes was nearly same because of the difference of bulk density.

ACKNOWLEDGMENTS. This research was supported by a grant(AB2-101) from Carbon Dioxide Reduction & Sequestration Research Center, one of the 21st Century Frontier Programs funded by the Ministry of Science and Technology of Korean government.

REFERENCES

1. R. Kumar, *Sep. Sci. and Tec.*, **1996**, *31*, 877.
2. G. Reiβ, *Gas Sep. & Purif.*, **1994**, *8*, 95.
3. Z. Budner, J. Dula, W. Podstawa and A. Gawdzik, *Trans IChemE*, **1999**, *77*, 405.
4. M. Kawai and T. Kaneko, *Gas Separation and Purification,* **1989**, *3*, 2.
5. J.-G. Jee, S.-J. Lee and C.-H. Lee, *Korean J. Chem. Eng*., **2004**, *21*, 1183.
6. S. Sircar and B.F. Hanley, *Sep. Sci. and Tech*., **1993**, *28*, 2553.
7. C-.T. Chou, D.-M. Ju and S.-C. Chang, *Sep. Sci. and Tech*., **1998**, *33*, 2059.
8. J. Jee, M. Park, S. Haam, and C.-H. Lee, *Sep. Sci. and Tech*., **2002**, *37*, 3465.
9. K.G. Teague, Jr. and T.F. Edgar, *Ind. Eng. Chem. Res.,* **1999**, *38*, 3761.
10. S. Farooq, R. D. M. Uthven and H. A. Boniface, *Chem. Eng. Sci*., **1989**, *44*, 2809.
11. B.-U. Choi, G.-M. Nam, D.-K. Choi, B.-K. Lee, S.-H. Kim and C.-H. Lee, *Korean J. Chem. Eng.* **2004**, *21*, 821.
12. N. Sundaram and P. C. Wankat, *Chem. Eng. Sci*., **1988**, *43*, 123
13. R. Rota and P. C. Wanket, *AIChE J*., **1990**, *36*, 1299.
14. J. Jee, J.-S. Lee and C.-H. Lee, *Ind. Eng. Chem. Res*., **2001**, *40*, 3647.
15. E. S. Kikkinides and R. T. Yang, *Chem. Eng. Sci*., **1993**, *48*, 1545.
16. J. Yang and C.-H. Lee, *AIChE J.,* **1998**, *44*, 1325.
17. T. W. Wever and R. K. Chakravort, *AIChE J*., **1974**, *20*, 228.
18. S. U. Rege and R. T. Yang, *Ind. Eng. Chem. Res*., **1997**, *36*, 5358.
19. A. Kapoor and R. T. Yang, *Chem. Eng. Sci*., **1989**, *44*, 1723.
20. G. A. Sorial, W. H. Granville and W. O. Daly, *Chem. Eng. Sci.*, **1983**, *38*, 1517.
21. A. Mendes, M. M. Costa, A. V. Carlos and A. E. Rodrigues, *Ind. Eng. Chem. Res*., **2000**, *39*, 138.
22. D. M. Ruthven, F. S. Arooq and K. S. Knaebel, "Pressure Swing Adsorption", VCH, New York, 1994.
23. R. T. Yang, "Gas separation by adsorption Processes", Butterworth, Boston, 1987.
24. S. U. Rege and R. T. Yang, *Chem. Eng. Sci.*, **2002**, *57*, 1139.
25. M. B. Kim, J. G. Jee, Y. S. Bae and C. -H. Lee, *Ind. Eng. Chem. Res.*, **2005**, *44*, 7208.
26. J. G. Jee, S. J. Lee, M. B. Kim and C. -H. Lee, *AIChE J*., **2005**, *52*, 2988.
27. S. Cavenati, C. A. Grande and A E. Rodrigues, *Chem. Eng. Sci.*, **2006**, *61*, 3893.